ACS Catalysis

Letter

pubs.acs.org/acscatalysis

Mn_5O_8 Nanoparticles as Efficient Water Oxidation Catalysts at Neutral pH

Donghyuk Jeong,[†] Kyoungsuk Jin,[†] Sung Eun Jerng,[†] Hongmin Seo,[†] Donghun Kim,[#] Seung Hoon Nahm,[‡] Sun Hee Kim,[#] and Ki Tae Nam*[,†]

[†]Department of Materials Science and Engineering, Seoul National University, Seoul 151-744, South Korea

[#]Western Seoul Center, Korea Basic Science Institute, Seoul, 120-140, Korea

[‡]Korea Research Institute of Standards and Science, Daejeon 305-340, Korea

Supporting Information

ABSTRACT: Mn_5O_8 nanoparticles (NPs) were obtained via the controlled oxidation of MnO NPs. The oxygen evolution reaction (OER) properties of Mn_5O_8 NPs were evaluated using cyclic voltammetry (CV). A current density of 5 mA/cm^2 was reached when 580 mV of overpotential was applied at pH 7.8. Electron paramagnetic resonance (EPR) analysis was conducted to investigate the origin of high OER activity of Mn_5O_8 NPs. From the EPR analysis, Mn^{3+} was found to be involved in the OER process of the Mn_5O_8 materials.

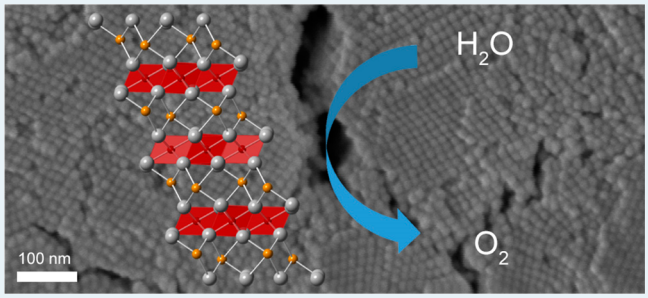

KEYWORDS: *water splitting, oxygen evolution reaction (OER), Mn_5O_8 nanoparticles, micron-sized Mn_5O_8, electrocatalyst*

Hydrogen energy has received substantial attention because hydrogen gas is environmentally friendly and has a high energy density. Currently, 96% of hydrogen energy is produced from gas reforming, which produces environmentally unfriendly byproducts, such as CO_2, making water splitting an attractive alternative method for hydrogen production. However, the oxygen evolution reaction (OER) hinders the water splitting reaction because its reaction kinetics are slower than that of the hydrogen evolution reaction (HER).[1] Therefore, a cost-effective and durable OER catalyst should be developed. In this regard, cobalt-based materials have been intensively studied as a water oxidation catalyst due to their low-cost, durability, and high activity. Their high activity can even be more enhanced through the combination with other supporting materials, such as gold, polymer, silica scaffold, and so forth.[1d,2]

On the other hand, many researchers have been investigating manganese-based catalysts because manganese is the only redox active component in the very efficient water oxidation complex (WOC) of photosystem II.[3] Thus, many researchers have studied Mn-based catalysts for water oxidation. The Driess group produced active MnO_x nanoparticles from inactive MnO nanoparticles using ceric ammonium nitrate (CAN) as the oxidant, and they showed that active MnO_x is more efficient than Mn_3O_4 but less efficient than Mn_2O_3.[4] The Dau group synthesized amorphous MnO_x film via electrodeposition, which is active under neutral conditions.[5] Kuo et al. fabricated a robust mesoporous Mn_2O_3 catalyst that has a high surface area and Mn^{3+} content.[6] Meng et al. showed that the crystallographic structure of catalyst affects its catalytic property by studying various polymorphs of MnO_2. They claimed that α-MnO_2 is the most efficient OER catalyst among the other MnO_2 phases due to its abundant di-μ-oxo bridges and the mixed valences.[7] The Nakamura group enhanced the OER properties of MnO_2 by stabilizing Mn^{3+} on the surface of MnO_2. As a result of this finding, Mn^{3+} is considered as an important species for efficient water oxidation.[8] Other researchers also suggested that Mn^{3+} affects the OER efficiency of the manganese oxide catalyst.[6,9]

Especially, the Rao group showed that Mn^{3+} is the water-oxidizing species because Mn^{3+} has the e_g^1 electron which is expected to give moderate bonding strength between O_2 and the catalyst required for high OER activity.[9b,10] In this context, our group reported a new pyrophosphate-based manganese catalyst, $Li_2MnP_2O_7$, and we observed the effect of Mn^{3+} on OER catalysis by tuning the Mn valence of the catalyst through delithiation.[9c] As described above, many manganese oxide electrocatalysts for OER have been reported. However, among these manganese oxide catalysts for OER, Mn_5O_8 has never been investigated.

Since Mn_5O_8 was first reported by W. Feitknecht in 1964,[11] interesting features of Mn_5O_8 have been discovered. Mn_5O_8 has a similar crystal structure to $Cd_2Mn_3O_8$[12] and $Ca_2Mn_3O_8$,[13] which is a highly asymmetric monoclinic structure. Also, it has the chemical formula of $Mn^{2+}{}_2Mn^{4+}{}_3O_8$, possessing a mixed Mn valency.[12a] Finally, Mn_5O_8 has a layered structure composed of

Received: April 8, 2015
Revised: June 23, 2015
Published: June 26, 2015

DOI: 10.1021/acscatal.5b01269
ACS Catal. 2015, 5, 4624−4628

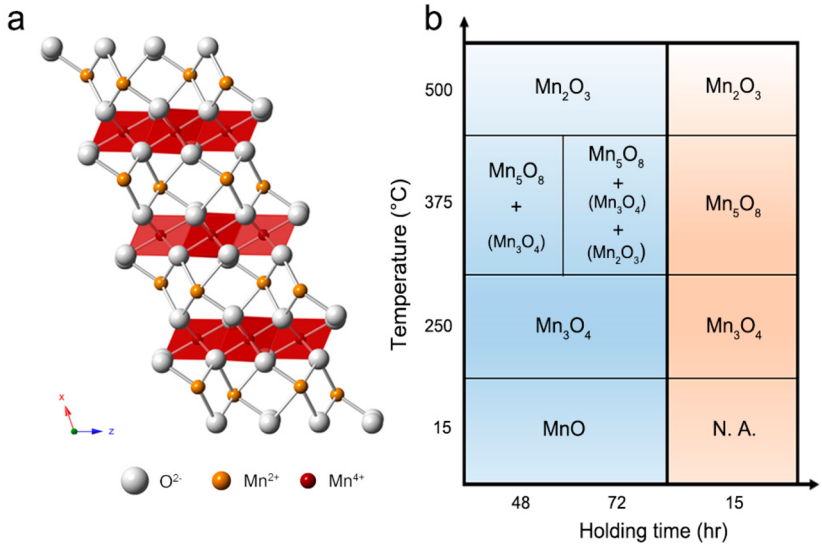

Figure 1. (a) Crystal structure of Mn_5O_8. (b) Synthesis conditions for various Mn-oxides (blue region: air atmosphere, red region: oxygen atmosphere).

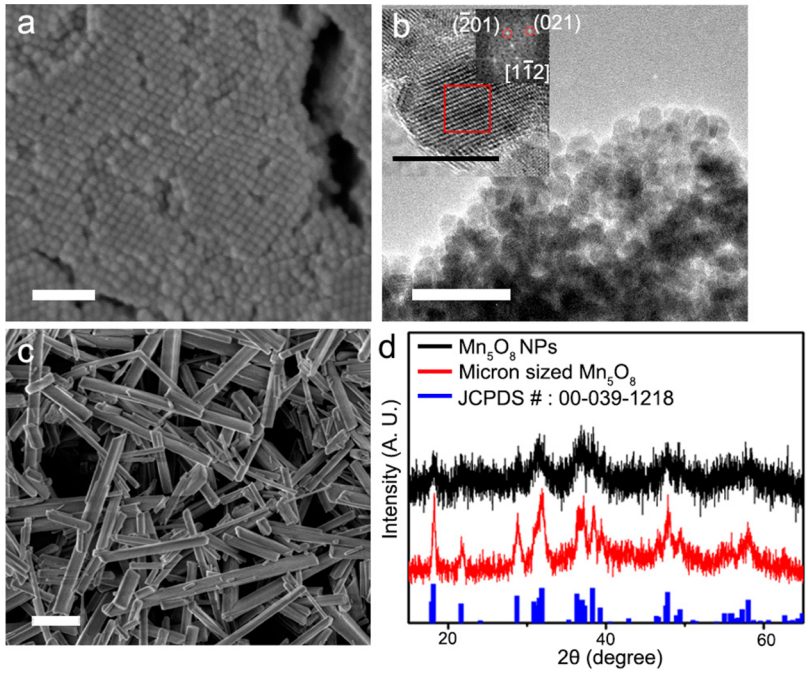

Figure 2. Characterization of Mn_5O_8. (a) SEM image of Mn_5O_8 NPs (scale bar: 100 nm). (b) TEM image of Mn_5O_8 NPs (scale bar: 50 nm, inset scale bar: 10 nm). (c) SEM image of micron-sized Mn_5O_8 (scale bar: 600 nm). (d) PXRD data of Mn_5O_8 materials.

a $[Mn_3O_8]^{4-}$ anionic layer with a MnO_6 octahedron and a Mn^{2+} cationic layer, which is shown in Figure 1a.[12b]

Interestingly, the features of Mn_5O_8 are expected to make Mn_5O_8 catalytically active for the OER. Tian et al. reported that the mixed valency of manganese oxide facilitates a redox reaction, which makes manganese oxide an active catalyst for the oxidation of alkanes.[14] Because a redox reaction is also involved in the water oxidation reaction, the mixed valency of Mn_5O_8 can make Mn_5O_8 an active catalyst for the OER.

In addition, there are many recent reports on layered materials, such as layered $NiFeO_x$, NiFe layered double hydroxide (LDH), ZnCo LDH, NiCo LDH, and CoMn LDH, which have high OER activities because of their high active area.[15]

Regarding asymmetric structure of Mn_5O_8, Jin et al. showed the high OER property of $Mn_3(PO_4)_2$-$3H_2O$ could be achieved due to its asymmetric crystal structure, which may facilitate Jahn−Teller distortion, thus stabilizing the Mn^{3+} species during the OER.[16] Therefore, we believe that Mn_5O_8 is a promising candidate as an OER catalyst. We synthesized Mn_5O_8 nanoparticles to maximize the catalytic ability and compared them with micron-sized Mn_5O_8.

In this study, we report the OER properties of Mn_5O_8 NPs for the first time. In addition, we demonstrate from EPR spectroscopic analysis that Mn^{3+} participates in the OER process of the Mn_5O_8 catalysts. Additionally, we found that the Mn^{3+} stability during the OER may affect the activity difference between the Mn_5O_8 NPs and the micron-sized Mn_5O_8.

DOI: 10.1021/acscatal.5b01269
ACS Catal. 2015, 5, 4624−4628

For the synthesis of the Mn_5O_8 NPs, 13 nm-sized spherical MnO NPs were first synthesized by a modified heat up method. (See Supporting Information for experimental details.) The phase and morphology of the MnO NPs were characterized using powder X-ray diffraction (PXRD), scanning electron microscopy (SEM), and transmission electron microscopy (TEM) analysis (Figures S1 and S3).

Then, MnO NPs were converted to Mn_5O_8 NPs via annealing under an oxygen atmosphere. To obtain Mn_5O_8 nanoparticles, we attempted various heat treatment conditions. As a result, we identified the optimal synthesis conditions of various Mn oxide phases starting from MnO NPs synthesized from our method (Figure 1b, S1). From the PXRD, SEM, and TEM analysis, it was shown that the obtained NPs were Mn_5O_8 (Figure 2b, inset; Figure 2d, black line), and there was no observable change in morphology or size after the heat treatment (Figure 2a,b). In contrast to other Mn oxides, Mn_2O_3 was obtained with a sintered morphology, resulting in sharp PXRD peaks.

Additionally, we synthesized micron-sized Mn_5O_8 as a reference material. The γ-MnOOH precursor was prepared using the hydrothermal method, and it was changed via a two-step heat treatment.[17] The phase and morphology of the precursor materials are shown in Figures S2 and S4. The obtained Mn_5O_8 compounds were rod-shaped with a micron-sized length and a 100 nm diameter (Figure 2c). The crystal structure was also confirmed using PXRD (Figure 2d, red line).

The activity of the Mn_5O_8 NPs for OER catalysis was evaluated using cyclic voltammetry (CV). The Mn_5O_8 NPs were prepared on a fluorine-doped tin oxide (FTO) glass substrate using spin coating. (See the Supporting Information for the cell preparation details.) The evaluation for OER activity was performed at pH 7.8 and in a 0.3 M sodium phosphate buffer solution. The high activity of the Mn_5O_8 NPs under near neutral conditions is displayed in Figure 3a. Because there are no previous reports on the OER properties of Mn_5O_8 NPs, we first confirmed that faradaic efficiency of Mn_5O_8 NPs is 92%, meaning that the measured current was originated from oxygen evolution (Figure S5). Then, we synthesized well-known catalysts, such as CoP_i and MnO_x, using the electrodeposition method, for comparison.[1d,5]

As shown in Figure 3a, the OER properties of the Mn_5O_8 NPs were similar to those of CoP_i and were markedly better than those of electrodeposited MnO_x. For the precise comparison, the OER properties of various electrocatalysts are summarized in Table S1, including noble metal oxide. To determine the catalytic stability of the Mn_5O_8 NPs, a bulk electrolysis (BE) experiment was conducted. The BE of Mn_5O_8 NPs over 5,000 s was recorded at 1.2 V vs Ag/AgCl. The black plateau line in Figure 3b shows that Mn_5O_8 NPs are relatively stable during the OER. To confirm the structural stability of Mn_5O_8 NPs during OER, we observed SEM and TEM image after bulk electrolysis. From the SEM image in Figure S6, it was shown that morphology of Mn_5O_8 NPs does not change during OER. In addition to that, Figure S7 shows that amorphization did not occur on the surface of Mn_5O_8 NPs. Further, FFT analysis of TEM image shows that the Mn_5O_8 phase was maintained, indicating high phase stability (Figure S7, inset). The CV stability of Mn_5O_8 NPs is also shown in Figure S8. When Nafion solution is added to prevent Mn_5O_8 NP detachment from the electrode, the Mn_5O_8 NPs showed improved stability at 1.3 V versus Ag/AgCl (red line in Figure 3b). We noted that the electrolysis curves of the Mn_5O_8 NPs with Nafion are slightly bumpy because of the oxygen bubbles produced during the OER.

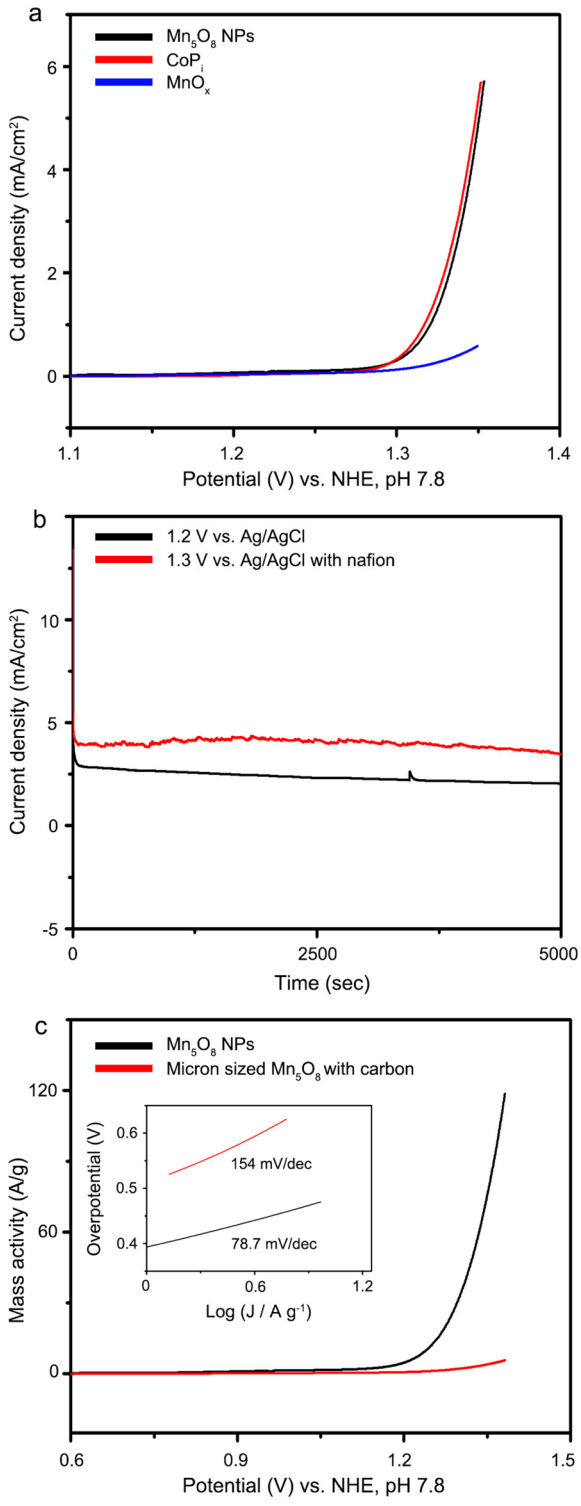

Figure 3. Electrochemical properties of the Mn_5O_8 NPs. (a) Polarization curves of Mn_5O_8 NPs, CoP_i and MnO_x at pH 7.8 in a 0.3 M phosphate buffer solution. (b) Bulk electrolysis curve of Mn_5O_8 NPs for 5000 s. (c) Mass activity comparison data between Mn_5O_8 NPs and micron-sized Mn_5O_8 with carbon (inset image: Tafel slope of Mn_5O_8 materials). Scan rate: 0.01 V/s.

The mass activity and the Tafel slope of the micron-sized Mn_5O_8 and Mn_5O_8 NPs were compared to investigate the

DOI: 10.1021/acscatal.5b01269
ACS Catal. 2015, 5, 4624−4628

effect of size on the catalytic properties (Figure 3c). To enhance electrical conductivity of micron-sized Mn_5O_8, we mixed micron-sized Mn_5O_8 with Vulcan carbon. Effect of Vulcan carbon on the mass activity of the micron-sized Mn_5O_8 is displayed in Figure S9. At the same overpotential (610 mV), the mass activity of the Mn_5O_8 NPs (116 A/g) was markedly higher than that of micron-sized Mn_5O_8 (5.7 A/g). To understand the origin of this activity difference, Brunauer–Emmett–Teller (BET) analysis was performed. The surface area of the Mn_5O_8 NPs and the rods was determined as 41.83 and 12.93 m^2/g, respectively. Although the Mn_5O_8 NPs have higher surface area than the micron-sized Mn_5O_8, the difference cannot fully explain the substantial activity difference between them. In addition, the Mn_5O_8 NPs had a lower Tafel slope (78.7 mV/dec) than the micron-sized Mn_5O_8 (154 mV/dec) (Figure 3c, inset), indicating that the Mn_5O_8 NPs are more efficient than the micron-sized Mn_5O_8 in the high potential region.

Thus, we thought that an intrinsic difference exists between the Mn_5O_8 NPs and the micron-sized Mn_5O_8. To reveal the origin of this intrinsic difference, we focused on the Mn(III) generation and stabilization in the materials because many researchers have reported the importance of Mn^{3+} during the OER in Mn-based electrocatalysts.[6,8,9,16] In previous reports emphasizing the importance of Mn(III), UV/vis and X-ray absorption spectroscopy (XAS) were used to detect the Mn(III) species.[5,8] In this study, EPR techniques were adopted to monitor the evolution of Mn(III) and its stabilization during the catalysis.

Catalyst ink with the same amount of Mn_5O_8 NPs and micron-sized Mn_5O_8 was loaded onto the FTO electrode to precisely compare them. We applied 1.25 V (vs Ag/AgCl) to the catalyst for 1000 s to observe the behavior of Mn^{3+} during the OER. Additionally, pyrophosphate (PP) solution was employed to prepare the EPR sample because PP is known as a redox-inactive material that can capture Mn^{3+} species.[8a,18] To prevent further electron transfer in the materials after OER, we froze each EPR sample with liquid nitrogen immediately after mixing the catalyst with other substances. (See the Supporting Information for preparation details.)

The X-band EPR spectra are recorded to show the behavior of Mn^{2+} and Mn^{3+} of Mn_5O_8 materials (Figure 4 and S10). As revealed in Figure S10a, typical Mn^{2+} EPR signal with the six-line splitting around 3413 G ($g \sim 2$) was detected in as-prepared Mn_5O_8 samples. Also, carbon radical signal appeared around 3440 G ($g \sim 2$) in the perpendicular mode EPR spectra because we mixed Vulcan carbon with catalysts to enhance electron transfer. (Perpendicular mode means microwave (H_1 field) and magnetic field (H_0 field) are perpendicular.)

Comparing Figure 4a with Figure S10a, Mn^{2+} of Mn_5O_8 disappears right after the OER. Mn^{3+} is shown from the six-line hyperfine splitting centered at 820 G ($g_{eff} \sim 8.2$) in the parallel mode EPR spectra. (Parallel mode means microwave (H_1 field) and magnetic field (H_0 field) are parallel.) The Mn^{3+} signal was enhanced immediately after the OER for both of the Mn_5O_8 materials (Figure 4b and Figure S10b). These results indicate that Mn^{3+} is involved in the OER process of Mn_5O_8. Importantly, there is a large difference in the Mn^{3+} EPR intensity between the Mn_5O_8 NPs and the micron-sized Mn_5O_8 right after OER as shown in Figure 4b. For the Mn_5O_8 NPs, strong and well-resolved six-line hyperfine splitting is shown; however, a weak and poorly resolved one occurs for the micron-sized Mn_5O_8, indicating that the Mn_5O_8 NPs have

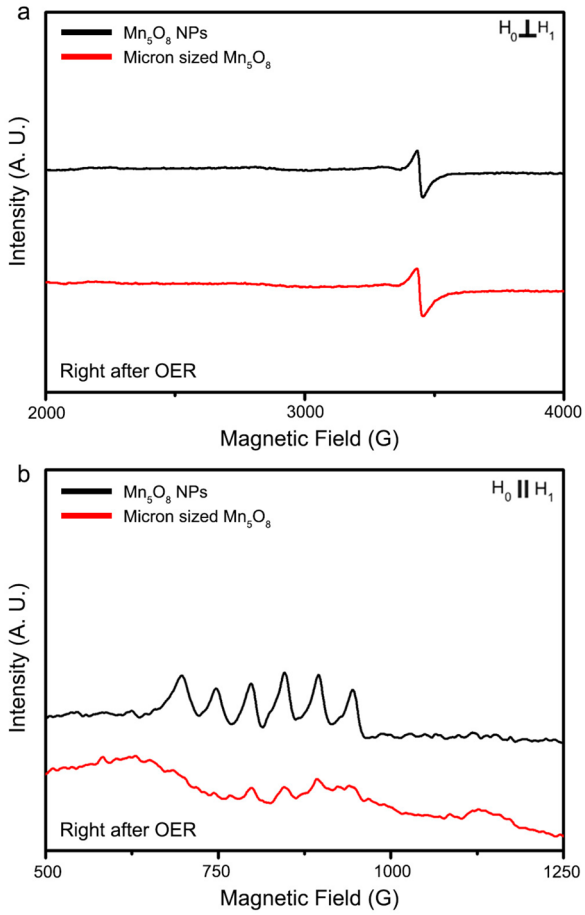

Figure 4. X-band EPR spectra of Mn_5O_8 materials following the OER. (a) Perpendicular mode for Mn^{2+} detection. (b) Parallel mode for Mn^{3+} detection.

much more Mn^{3+} species during the OER. This result shows that Mn^{3+} is more stable intrinsically in the Mn_5O_8 NPs. We think that the higher catalytic activity of Mn_5O_8 NPs may be due to the improved stability of Mn^{3+} along with the increased surface area.

In conclusion, we successfully developed a method to obtain uniform 13 nm Mn_5O_8 NPs. For Mn_5O_8 NPs, the overpotential to reach 5 mA/cm^2 is only 580 mV, which is comparable to that of the well-known CoP_i. The robust catalytic stability of Mn_5O_8 NPs is also confirmed. This is the first report on the OER properties of Mn_5O_8 NPs under near neutral conditions. Using EPR analysis, we observed that Mn^{3+} participates in the OER process of the Mn_5O_8 materials. We also observed that the Mn_5O_8 NPs showed superior catalytic activity compared with microparticles. On the basis of the EPR data showing the high Mn^{3+} content during OER, we believe that the increased catalytic activity may be attributed to the stabilization of Mn^{3+} in the Mn_5O_8 NPs.

■ ASSOCIATED CONTENT

Supporting Information

The Supporting Information is available free of charge on the ACS Publications website at DOI: 10.1021/acscatal.5b01269.

Experimental section; XRD and SEM image of precursor of Mn_5O_8 materials; Faradaic efficiency determination; SEM and TEM analysis after OER; CV curve of Mn_5O_8

DOI: 10.1021/acscatal.5b01269
ACS Catal. 2015, 5, 4624–4628

NPs; Effect of Vulcan carbon on mass activity; EPR result of as-prepared Mn_5O_8 materials (PDF)

AUTHOR INFORMATION

Corresponding Author

*E-mail: nkitae@snu.ac.kr.

Notes

The authors declare no competing financial interest.

ACKNOWLEDGMENTS

This work was supported by the Basic Science Research Program (2011-0011225, 2011-0017587, 2012M3A7B4049807), the Global Frontier R&D Program of the Center for Multiscale Energy System (2011-0031574) and the Fusion Research Program for Green Technologies through the National Research Foundation of Korea (2012M3C1A1048863) funded by the Ministry of Science, ICT and Future, Korea. This research was also supported by the Ministry of Science, ICT and Future, through the Research Institute of Advanced Materials (RIAM) to K.T.N. and The National Research Council of Science and Technology through the Degree & Research Center Program (DRC-14-3-KBSI) to S.H.K.

REFERENCES

(1) (a) Hocking, R. K.; Brimblecombe, R.; Chang, L.-Y.; Singh, A.; Cheah, M. H.; Glover, C.; Casey, W. H.; Spiccia, L. *Nat. Chem.* **2011**, *3*, 461−466. (b) Rossmeisl, J.; Qu, Z.-W.; Zhu, H.; Kroes, G.-J.; Nørskov, J. K. *J. Electroanal. Chem.* **2007**, *607*, 83−89. (c) Suntivich, J.; May, K. J.; Gasteiger, H. A.; Goodenough, J. B.; Shao-Horn, Y. *Science* **2011**, *334*, 1383−1385. (d) Kanan, M. W.; Nocera, D. G. *Science* **2008**, *321*, 1072−1075. (e) Sim, U.; Yang, T.-Y.; Moon, J.; An, J.; Hwang, J.; Seo, J.-H.; Lee, J.; Kim, K. Y.; Lee, J.; Han, S. *Energy Environ. Sci.* **2013**, *6*, 3658−3664. (f) Sim, U.; Moon, J.; An, J.; Kang, J. H.; Jerng, S. E.; Moon, J.; Cho, S.-P.; Hong, B. H.; Nam, K. T. *Energy Environ. Sci.* **2015**, *8*, 1329−1338.

(2) (a) Zhang, G.; Zang, S.; Wang, X. *ACS Catal.* **2015**, *5*, 941−947. (b) Jiao, F.; Frei, H. *Energy Environ. Sci.* **2010**, *3*, 1018−1027. (c) Fominykh, K.; Feckl, J. M.; Sicklinger, J.; Döblinger, M.; Böcklein, S.; Ziegler, J.; Peter, L.; Rathousky, J.; Scheidt, E. W.; Bein, T. *Adv. Funct. Mater.* **2014**, *24*, 3123−3129. (d) Smith, R. D. L.; Prévot, M. S.; Fagan, R. D.; Trudel, S.; Berlinguette, C. P. *J. Am. Chem. Soc.* **2013**, *135*, 11580−11586. (e) Yeo, B. S.; Bell, A. T. *J. Am. Chem. Soc.* **2011**, *133*, 5587−5593.

(3) Umena, Y.; Kawakami, K.; Shen, J.-R.; Kamiya, N. *Nature* **2011**, *473*, 55−60.

(4) (a) Indra, A.; Menezes, P. W.; Zaharieva, I.; Baktash, E.; Pfrommer, J.; Schwarze, M.; Dau, H.; Driess, M. *Angew. Chem., Int. Ed.* **2013**, *52*, 13206−13210. (b) Menezes, P. W.; Indra, A.; Littlewood, P.; Schwarze, M.; Göbel, C.; Schomäcker, R.; Driess, M. *ChemSusChem* **2014**, *7*, 2202−2211.

(5) Zaharieva, I.; Chernev, P.; Risch, M.; Klingan, K.; Kohlhoff, M.; Fischer, A.; Dau, H. *Energy Environ. Sci.* **2012**, *5*, 7081−7089.

(6) Kuo, C.-H.; Mosa, I.; Poyraz, A. S.; Biswas, S.; El-Sawy, A. M.; Song, W.; Luo, Z.; Chen, S.-Y.; Rusling, J. F.; He, J. *ACS Catal.* **2015**, *5*, 1693−1699.

(7) Meng, Y.; Song, W.; Huang, H.; Ren, Z.; Chen, S.-Y.; Suib, S. L. *J. Am. Chem. Soc.* **2014**, *136*, 11452−11464.

(8) (a) Takashima, T.; Hashimoto, K.; Nakamura, R. *J. Am. Chem. Soc.* **2011**, *134*, 1519−1527. (b) Takashima, T.; Hashimoto, K.; Nakamura, R. *J. Am. Chem. Soc.* **2012**, *134*, 18153−18156.

(9) (a) Robinson, D. M.; Go, Y. B.; Mui, M.; Gardner, G.; Zhang, Z.; Mastrogiovanni, D.; Garfunkel, E.; Li, J.; Greenblatt, M.; Dismukes, G. C. *J. Am. Chem. Soc.* **2013**, *135*, 3494−3501. (b) Maitra, U.; Naidu, B.; Govindaraj, A.; Rao, C. *Proc. Natl. Acad. Sci. U. S. A.* **2013**, *110*, 11704−11707. (c) Park, J.; Kim, H.; Jin, K.; Lee, B. J.; Park, Y.-S.; Kim, H.; Park, I.; Yang, K. D.; Jeong, H.-Y.; Kim, J.; Hong, K. T.; Jang, H. W.; Kang, K.; Nam, K. T. *J. Am. Chem. Soc.* **2014**, *136*, 4201−4211. (d) Jin, K.; Chu, A.; Park, J.; Jeong, D.; Jerng, S. E.; Sim, U.; Jeong, H.-Y.; Lee, C. W.; Park, Y.-S.; Yang, K. D. *Sci. Rep.* **2015**, *5*, 10279.

(10) Naidu, B.; Gupta, U.; Maitra, U.; Rao, C. *Chem. Phys. Lett.* **2014**, *591*, 277−281.

(11) Feitknecht, W. Einfluss der Teilchengrösse auf den Mechanismus von Festkörperreaktionen. *Pure Appl. Chem.* **1964**, *9*, 423−440.

(12) (a) Oswald, H.; Feitknecht, W.; Wampetich, M. *Nature* **1965**, *207*, 72−72. (b) Oswald, H.; Wampetich, M. *Helv. Chim. Acta* **1967**, *50*, 2023−2034.

(13) Ansell, G. B.; Modrick, M. A.; Longo, J.; Poeppeimeler, K.; Horowitz, H. *Acta Crystallogr., Sect. B: Struct. Crystallogr. Cryst. Chem.* **1982**, *38*, 1795−1797.

(14) Tian, Z.-R.; Tong, W.; Wang, J.-Y.; Duan, N.-G.; Krishnan, V. V.; Suib, S. L. *Science* **1997**, *276*, 926−930.

(15) (a) Trotochaud, L.; Ranney, J. K.; Williams, K. N.; Boettcher, S. W. *J. Am. Chem. Soc.* **2012**, *134*, 17253−17261. (b) Gong, M.; Li, Y.; Wang, H.; Liang, Y.; Wu, J. Z.; Zhou, J.; Wang, J.; Regier, T.; Wei, F.; Dai, H. *J. Am. Chem. Soc.* **2013**, *135*, 8452−8455. (c) Zou, X.; Goswami, A.; Asefa, T. *J. Am. Chem. Soc.* **2013**, *135*, 17242−17245. (d) Song, F.; Hu, X. *J. Am. Chem. Soc.* **2014**, *136*, 16481−16484.

(16) Jin, K.; Park, J.; Lee, J.; Yang, K. D.; Pradhan, G. K.; Sim, U.; Jeong, D.; Jang, H. L.; Park, S.; Kim, D.; Sung, N.-E.; Kim, S. H.; Han, S.; Nam, K. T. *J. Am. Chem. Soc.* **2014**, *136*, 7435−7443.

(17) Gao, T.; Norby, P.; Krumeich, F.; Okamoto, H.; Nesper, R.; Fjellvåg, H. *J. Phys. Chem. C* **2009**, *114*, 922−928.

(18) (a) Klewicki, J.; Morgan, J. *Geochim. Cosmochim. Acta* **1999**, *63*, 3017−3024. (b) Klewicki, J. K.; Morgan, J. J. *Environ. Sci. Technol.* **1998**, *32*, 2916−2922.

DOI: 10.1021/acscatal.5b01269
ACS Catal. 2015, 5, 4624−4628